EES Solar

PAPER

View Article Online
View Journal | View Issue

Cite this: *EES Sol.*, 2025, **1**, 645

Modeling the FA and I losses in mixed-halide perovskite through chemical rate equations: insights into light-induced degradation†

Jeremy Hieulle, [a] Anurag Krishna, [bcd] Hazem Adel Musallam, [a] Tom Aernouts [bcd] and Alex Redinger *[a]

Photo-induced degradation is a major obstacle for the practical use of perovskites in solar cells, and understanding this degradation is key to maximizing the potential of perovskite photovoltaics. This study addresses the lack of accurate models for photochemical degradation kinetics in perovskites by deriving rate equations for a cutting-edge triple-cation mixed halide perovskite using a two-step reaction model. Our model describes the temporal evolution of iodine and formamidinium losses, along with the generation of metallic lead (Pb(0)) under continuous white light. Applied to perovskite samples with varying bromine contents (5 to 20%), we found that increased Br content enhances stability under illumination, aligning with reports for Br contents below 25%. Additionally, our study shows that degradation pathways vary between nitrogen (N_2) and ultra-high vacuum (UHV) environments. UHV conditions accelerate Pb(0) formation, while no Pb(0) appears in N_2. Despite the absence of Pb(0) in N_2, atomic force microscopy data reveal light-induced degradation, contradicting previous claims of N_2 stability. This degradation includes perovskite's transformation into lead-iodide and granular structure development on the surface. These findings improve understanding of environmental impacts on perovskite stability and highlight XPS's limitations in detecting photodegradation in N_2.

Received 9th April 2025
Accepted 7th July 2025

DOI: 10.1039/d5el00058k

rsc.li/EESSolar

Broader context

The urgent need for sustainable energy solutions has never been more critical, as the reliance on fossil fuels contributes significantly to climate change and global warming. Solar energy, one of the most abundant resources, presents a promising avenue to mitigate these challenges. This research focuses on perovskite materials, which have emerged as a leading alternative to traditional silicon solar panels due to their potential for lower production costs and flexible applications. However, issues such as premature degradation and species migration hinder their commercialization. Our study, conducted within the LION (LIght ON perovskite) project funded by FNR, investigates the impact of light on the degradation of perovskite. By employing a kinetic rate equation model, we revealed that perovskite films with optimized bromine content exhibit enhanced stability, shifting the degradation pathways under varying environmental conditions. These findings not only improve understanding of the degradation mechanisms but also pave the way for developing filters that can enhance the longevity of perovskite solar panels. Ultimately, this research contributes to the advancement of cost-effective, stable, and efficient solar technologies essential for the transition to a more sustainable energy future and the reduction of greenhouse gas emissions.

1 Introduction

Over the past decade, perovskites have garnered significant attention for their possible application in solar cell technology. In just a few years, they have achieved power conversion efficiencies that compete with those of the well-established silicon technology, currently reaching 26.7% for single-junction cells and 33.9% for tandem cells.[1,2] Despite their high efficiency, several factors, including, temperature, water, oxygen, and light, have been shown to impede the long-term stability of perovskite-based solar cell devices.[3–8] While encapsulation can address the instability caused by oxygen and water,[9] the instability caused by light remains a more concerning issue for solar cells. It has been proposed that both the high efficiency and low stability of perovskites are linked to long-lasting hot carriers,[10,11] which allow for efficient charge extraction but also promote undesirable chemical reactions leading to the material's intrinsic degradation. Several reaction pathways have been suggested to explain the photochemical degradation of perovskite absorber materials.[3,10,12–20] The reaction pathway that has gained consensus within the community so far involves a two-stage process: initially, the perovskite decomposes into lead

[a]*Department of Physics and Materials Science, University of Luxembourg, Luxembourg City L-1511, Luxembourg. E-mail: jeremy.hieulle@uni.lu; alex.redinger@uni.lu*
[b]*Thin Film PV Technology, Imec, Imo-imomec, Thor Park 8320, Genk 3600, Belgium*
[c]*Energy Ville, Imo-imomec, Thor Park 8320, Genk 3600, Belgium*
[d]*Hasselt University, Imo-imomec, Martelarenlaan 42, Hasselt 3500, Belgium*

† Electronic supplementary information (ESI) available. See DOI: https://doi.org/10.1039/d5el00058k

iodide,[21,22] and then in the second step, this lead iodide further breaks down into metallic lead.[12,23,24] Illumination has also been found to trigger ion migration within the cell.[25–28] This migration can result in undesirable chemical reactions and phase segregation, both of which contribute to a decrease in the efficiency of the perovskite cell. Some of these losses are reversible when the perovskite is placed in the dark.[29,30]

Despite significant attention given to light-induced photochemical degradation processes, no studies have yet focused on accurately modeling the time evolution (kinetics) of this photochemical degradation phenomenon. Understanding the rate of photochemical degradation, particularly the rates of iodine and FA losses, along with the rate of the chemical reaction producing metallic lead (Pb(0)), is essential for thoroughly comprehending the light-induced degradation of perovskite materials and for developing mitigation strategies. Cappel *et al.*[31] showed that light could trigger the generation of metallic lead (Pb(0)) at the perovskite surface due to chemical decomposition. The presence of Pb(0) was detected by XPS even after a short illumination time.[31–33] Several reports in the literature[32,34–37] have suggested that placing perovskite in an inert N_2 environment could suppress perovskite degradation by quenching ion migration.

In this study, we derived the rate equations for the photo-induced chemical degradation of a state-of-the-art triple cation hybrid organic–inorganic halide perovskite, utilizing a two-step chemical reaction model. We tested our model to fit the data of the temporal evolution of iodine(I) and formamidinium (FA) losses, as well as the generation of metallic lead (Pb(0)), under continuous white light illumination. We demonstrate that our model can be used to accurately describe the photochemical degradation of three perovskite $Cs_{0.05}FA_{0.85}MA_{0.10}Pb(I_{1-x}Br_x)_3$ samples containing 5 to 20% of bromine (*e.g.* $x = 0.05$; $x = 0.20$, respectively). Our model shows that elevating the Br content in mixed halide perovskite enhances the material's stability when exposed to light. These findings agree with several reports in the literature, where it was found that Br is beneficial to the stability of mixed halide perovskite (for Br content <25%).[38–41] More intriguingly, by employing our rate equation model, we discovered that the photochemical degradation pathway varies depending on the environmental conditions, whether it is nitrogen (N_2) or ultra-high vacuum (UHV), even though both environments are considered to be inert. Under UHV conditions, the photochemical reaction resulting in the formation of metallic lead proceeds at an accelerated rate. In contrast, if the samples are exposed to light in an N_2 environment, we did not find any metallic lead in the XPS. However, in an N_2 environment, light-induced degradation continues to occur. Particularly the transformation of perovskite into detrimental lead-iodide (PbI_2), as well as into under-stoichiometric PbI_x domains continues to proceed at a rate comparable to that in a vacuum. These findings of a photo-chemical decomposition of perovskite in N_2 are in contradiction with several reports in the literature, where no degradation was observed. These studies have been mainly based on XPS measurements. Here we show that XPS is mostly insensitive to the perovskite photodegradation in N_2 due to the absence of the Pb(0) signal (in contrast to the degradation in a vacuum). Here, by employing our rate equation model, we could analyze in detail the FA and I losses in N_2, enabling us to demonstrate that photodegradation does occur even in N_2. Our atomic force microscopy (AFM) measurements show the formation of granular structures at the material's surface due to the light exposure for both N_2 and vacuum environments.

2 Results and discussion

2.1 Rate equations and the two-step model of perovskite photochemical degradation

Previous reports have demonstrated that X-ray photoelectron spectroscopy (XPS) and scanning probe microscopy (SPM) are valuable tools for monitoring light-induced degradation in hybrid organic-inorganic halide perovskite.[39,42–45] Here we used XPS to follow the photochemical degradation of a state-of-the-art $Cs_{0.05}FA_{0.85}MA_{0.10}Pb(I_{0.95}Br_{0.05})_3$ triple-cation and mixed halide perovskite film (300 nm thick) fabricated *via* a solution process (spin-coating). This absorber material was successfully employed to fabricate solar cell devices (Fig. S1 and S2†), with relatively high efficiency (Table I in the ESI†). Due to XPS's relatively narrow probing depth (around 10 nm deep), our photo-degradation study focuses on the half-cell architecture (Fig. S3†).

In our previous research work[46] we demonstrated that the increase in the metallic lead signal (*e.g.*, Pb in a zero oxidation state, later referred to as Pb(0)) observed in XPS under illumination can be used to monitor the degradation of perovskite over time. In the same work, we demonstrated that light induces the generation of granular phases (PbI_x, with $x < 2$) at the surface of the perovskite material that could be detected by atomic force microscopy and Kelvin probe force microscopy (KPFM).

The novel approach of this work involves developing a rate equation model that not only tracks the generation of metallic lead but also reproduces the loss of iodine(I) and formamidiium (FA) under continuous light exposure, as a function of halide ratio, and environmental conditions. Furthermore, unlike our previous study, we utilized the coverage of the granular structure recorded in the AFM/KPFM maps to predict light-induced losses of I^- and FA^+, in the absence of a Pb(0) signal in the XPS.

Fig. 1 illustrates the XPS, AFM, and KPFM results for a perovskite film containing 5% Br, showing its degradation after being exposed to either darkness or continuous white light for 56 hours. A halogen lamp was used to provide illumination, with an irradiance of 16 mW cm^{-2} (0.16 sun). Fig. 1a shows the Pb4f core level measured by XPS for the pristine perovskite sample kept in the dark. The perovskite Pb4f core level spectrum consists of two doublet peaks. The first doublet peak, located at 138.5 and 143.4 eV, is associated with spin–orbit coupling split peaks of lead in the +2 oxidation state, referred to as Pb(2+). The second doublet peak at a lower binding energy (137.2 eV and 142.1 eV) is linked to lead in a zero oxidation state, *e.g.* metallic lead, denoted as Pb(0). As described in a previous study, the Pb(2+) state is associated with unperturbed

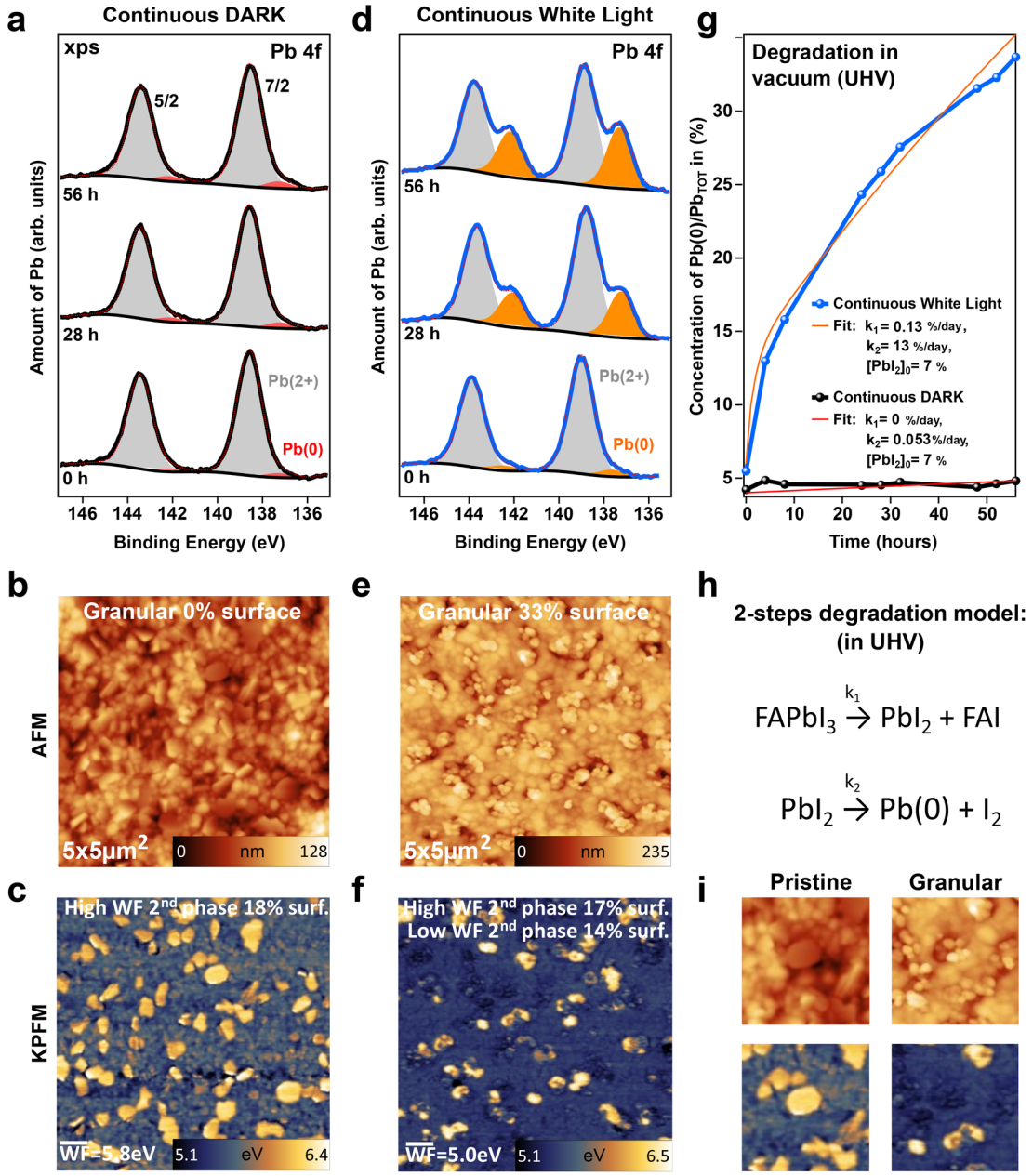

Fig. 1 Light-induced chemical degradation in hybrid organic–inorganic halide perovskite: (a–c) The oxidation state of lead, the surface topography, and the surface work function of a pristine triple-cation $Cs_{0.05}FA_{0.85}MA_{0.10}Pb(I_{0.95}Br_{0.05})_3$ perovskite film kept in the dark measured respectively by XPS, AFM and KPFM. For the pristine sample, a negligible signal of metallic lead (Pb(0)) was recorded in the XPS, accompanied by a well-defined and smooth grain in the AFM image. Typical high work-function domains are observed in the KPFM map due to a slight PbI_2 excess in the growth conditions. (d–f) The Pb4f core level, the surface topography, and the work function map of a similar perovskite sample exposed to 56 hours of continuous white light illumination. After light exposure, a huge increase in the Pb(0) signal is observed. This is accompanied by the appearance of a small granular structure on the surface topography (e), while the high work-function domains related to PbI_2 are disappearing (f). The evolution of the Pb(0) signal in XPS as a function of time and illumination conditions is plotted in (g). The blue curve corresponds to the light-exposed sample, while the black curve corresponds to the sample kept in the dark. A two-step degradation model with rate equations (h) can be built to describe the photo-chemical changes in the sample. The results of the fit of the first-order chemical rate equation are plotted in (g) as orange and red solid lines for the sample exposed to light and kept in the dark, respectively. (i) Enlarged AFM and KPFM maps of a pristine domain and light-degraded granular domain (image size: 1.6 × 1.6 μm^2).

pristine perovskite, while Pb(0) corresponds to the degraded perovskite compound. By tracking the evolution of the amount of Pb(2+) and Pb(0) signals, it is therefore possible to track the degradation of the perovskite film.

Fig. 1a shows that the amount of Pb(2+) and Pb(0) is constant over time for the whole 56 h of measurements, suggesting that the perovskite film is stable in the dark in ultra-high vacuum (UHV). This claim is further supported by AFM and KPFM

measurements, where no substantial change was observed with respect to a freshly grown pristine perovskite film (Fig. S12a–c†). After 56 h in the dark and in a vacuum, the perovskite surface topography measured by AFM is still composed of well-defined and smooth grains (Fig. 1b), similar to that in the pristine unperturbed case. In addition, the KPFM map displays the typical electronic landscapes with two work function domains (Fig. 1c), as is usually observed for this type of perovskite that was grown with a slight PbI_2 excess. The domains with a higher work function in the KPFM map (*e.g.* bright yellow domains) correspond to the PbI_2 domains, while the lower work function domains are associated with the $Cs_{0.05}FA_{0.85}MA_{0.10}Pb(I_{0.95}Br_{0.05})_3$ perovskite film.

In contrast, if the sample is exposed to continuous white light, a strong increase in the Pb(0) signal is observed over time (orange peak, in Fig. 1d), demonstrating the photochemical degradation of the perovskite film leading to the generation of metallic lead. It is important to note that the X-ray source parameters (power, exposure time, and X-ray dose) were kept strictly the same for both measurements in the dark and under light illumination, enabling us to rule out X-rays as the cause of the degradation. Moreover, after 56 h of continuous light exposure, strong morphological changes are observed in the AFM topographic image of the perovskite, where granular structures appear at the surface (Fig. 1e). These light-induced granular structures have been observed and identified in our previous work[46] and are related to the degradation of the perovskite into under-stoichiometric PbI_x, with $x < 2$. These small granular structures cover 33% of the surface, while they were completely absent in the perovskite film kept in the dark as well as in pristine perovskite. In addition, the electronic landscape measured by KPFM shows a reduction of the work function at the positions of the granular structures (Fig. 1f). The PbI_2 domains seem to have been eaten up during the degradation process. Both the chemical changes observed in XPS and the morphological and electronic changes observed by AFM and KPFM point toward a light-induced chemical degradation of the perovskite film and of PbI_2.

Therefore, we conclude that the perovskite film is chemically unstable against continuous white light exposure in UHV. This finding becomes even more apparent in Fig. 1g, where we plotted the concentration of Pb(0) as a function of time for both the perovskite sample kept in the dark (black curve) and the perovskite sample exposed to continuous white light (blue curve).

To reproduce the time evolution of Pb(0) under white light in our triple cation mixed-halide perovskite ($Cs_{0.05}FA_{0.85}MA_{0.10}Pb(I_{0.95}Br_{0.05})_3$), we have derived rate equations by considering the first order chemical reaction. Based on previous reports in the literature[47,48] on the possible reaction paths we have used a simplified 2-step model (Fig. 1h).

In the first chemical reaction step (1), the perovskite material is decomposed into lead diiodide (PbI_2) and formamidinium iodide (FAI).

$$FAPbI_3 \xrightarrow{k_1} PbI_2 + FAI \quad (1)$$

In the second chemical reaction step (2), the lead iodide is converted to metallic lead, inducing a reduction of Pb from a (+2) oxidation state to a 0 oxidation state. This explains the increase in the Pb(0) signal recorded in XPS under white light exposure.

$$PbI_2 \xrightarrow{k_2} Pb(0) + I_2 \quad (2)$$

For each of these two steps (1) and (2), we can attribute a reaction rate (speed of the reaction), namely k_1 and k_2. By considering first-order chemical reactions, we can then derive an equation for the time evolution of the amount of Pb in the oxidation state 0:

$$[Pb(0)]_t = 1 - \left([PbI_2]_0 \cdot e^{-k_2 t} + \frac{[FAPI]_0 \cdot k_1}{k_2 - k_1} \left(e^{-k_1 t} - e^{-k_2 t} \right) + [FAPI]_0 e^{-k_1 t} \right) \quad (3)$$

Eqn (3) was previously derived in one of our earlier studies,[46] and a detailed mathematical derivation is also presented in the ESI.† The result of our 2-step photochemical degradation model is depicted as a fit to the curves in Fig. 1g. The values extracted for the reaction rates are displayed in the inset of Fig. 1g. It is found that k_1 and k_2 are several orders of magnitudes smaller for the perovskite kept in the dark as compared to those for the perovskite exposed to continuous white light. More importantly, k_1 is nearly zero in the dark, emphasizing that the conversion of the perovskite is a light-induced process.

Eqn (3) assumes a pure $FaPbI_3$ compound which decomposes into PbI_2 and FAI. However, this is not the case here since we carried out our study on the complex triple cation mixed-halide perovskite ($Cs_{0.05}FA_{0.85}MA_{0.10}Pb(I_{0.95}Br_{0.05})_3$). Therefore, the validity of the rate equation can be questioned. To determine if the formalism applies to our perovskites as well, we conducted additional experiments, which are explained in the following sections. The triple cations are mainly composed of $FAPbI_3$ (up to 85% of the sample), and therefore the first chemical reaction step is expected to be dominated by the degradation of $FAPbI_3$ into lead diiodide, while the second reaction step is dominated by the transformation of PbI_2 into metallic lead. However, one might argue that the Pb(0) generation could be obtained instead from the decomposition of lead bromide ($PbBr_2$) into metallic lead. To check this possibility, we have investigated the light-induced degradation of pure PbI_2 and $PbBr_2$ films and compared the rate at which they are converted into Pb(0). We found that the PbI_2 film degraded at a much faster rate than $PbBr_2$ under the same light illumination conditions (7 times faster, see ESI Fig. S4†). This means that, even though $PbBr_2$ can indeed degrade into Pb(0), it is not the main contributor to the metallic lead signal measured in Fig. 1g. It accounts for only 1% of the total Pb(0) measured after 56 h (*e.g.* 33%), with the remainder (*e.g.*, 32%) resulting from the decomposition of lead iodide (PbI_2).

Similarly, one might argue that our current model does not explicitly account for the degradation of $MAPbI_3$ into MAI and

PbI_2. Nevertheless, considering that our perovskite composition includes only 10% $MAPbI_3$ and 85% $FAPbI_3$, with experimental observations showing a 34% generation of Pb(0) after 56 hours under white light, the contribution of $MAPbI_3$ decomposition is assumed to be minor. As even complete decomposition of $MAPbI_3$ would only account for a 10% increase in Pb(0), it is evident that the majority of Pb(0) results from $FAPbI_3$ decomposition into FAI and PbI_2. Therefore, we initially omitted $MAPbI_3$ degradation in our model fitting.

Using a similar methodology as the one described by Zhao *et al.*,[49] we can estimate the lowering of the activation energy for the perovskite degradation under light as compared to dark conditions ($\Delta E_a = E_{a,dark} - E_{a,light}$). This is achieved through the following equation:

$$\Delta E_a = k_B T \times \ln(AF) \quad (4)$$

where AF represents the acceleration factor, defined as the ratio of the reaction rates under light and dark conditions ($k_{2,light}/k_{2,dark}$). The full derivation of eqn (4) is provided in the ESI.†

By applying eqn (4) with $T = 300$ K and the k_2 values for both light and dark conditions, we found an acceleration factor AF = 245 and ΔE_a = 142 meV. Thus, the activation energy for perovskite degradation is 142 meV lower under light conditions compared to dark conditions.

So far, the analysis is analogous to ref. 46 It is interesting to note that although the samples were prepared in different laboratories with different synthesis methods, the rate constants k_1 and k_2 are very similar. This shows that the model is quite general and is not specific to one type of perovskite. We do not claim that our model completely encompasses all the mechanisms involved in light-induced degradation. It's likely that conversion into PbI_2 isn't the sole pathway for perovskite degradation, as various studies have proposed different reaction pathways.[3,10,12–20] Nonetheless, our model offers a clear and effective kinetic framework that successfully models the time evolution of degradation byproducts in perovskites under external illumination stress.

Previous reports have suggested that X-rays could also trigger perovskite degradation.[50,51] Here, we do not claim that radiolysis is entirely absent during XPS measurements. However, we clearly demonstrate that the variation in Pb(0) is primarily caused by exposure to white light. This explains the significant differences in behavior observed with and without white light, despite the X-ray exposure remaining constant.

In the next step, we will go one step further and analyze the losses of FA and I too, which should allow us to further refine our kinetic model of light-induced degradation.

2.2 Iodine and FA losses under light exposure

Our two-step chemical rate equation model allows us to estimate the losses of iodine and FA over time. A careful examination of eqn (1) and (2) reveals that for each Pb(0) produced, one FAI and one I_2 molecule are released from the perovskite. FAI and I_2 are known for their volatile nature. Assuming that all FAI and I_2 generated during the photodegradation desorb from the sample at a rate faster than k_1 and k_2, it is possible to derive separate rate equations for FA and I.

Considering eqn (1), it follows that FA losses must be exclusively related to the rate k_1, such as:

$$[FA]_t = [FA]_0 + [FAPI]_0(e^{-k_1 t} - 1) \quad (5)$$

Similarly, considering eqn (1) and (2), it follows that every time Pb(0) is generated, three iodine molecules are released (lost). Therefore, the time evolution of iodine can be derived from the Pb(0) time evolution as:

$$[I]_t = [I]_0 - 3 \times ([Pb(0)]_t - [Pb(0)]_0) \quad (6)$$

The full derivation of eqn (5) and (6), is given in the ESI.†

Based on the rate eqn (5) and (6), and based on the time evolution of Pb(0) generation, it is then possible to reproduce the time evolution of FA and iodine losses due to the photochemical degradation of the perovskite.

Fig. 2 depicts the evolution of iodine, FA and Pb(0) content in our perovskite material ($Cs_{0.05}FA_{0.85}MA_{0.10}Pb(I_{0.95}Br_{0.05})_3$) over time as a function of illumination conditions. The FA signal was extracted from the N1s spectra measured by XPS, and was deconvoluted from the MA signal based on its distinct binding energy (Fig. S5†). The 2-step degradation model depicted by the solid orange line in Fig. 2, corresponds to the results of eqn (5) and (6). Within the measurement error, the perovskite does not degrade in UHV in the dark. The amount of metallic lead does not increase over time in the dark (Fig. 2a), and the k_1 and k_2 rates are negligible. Since k_1 and k_2 are small in the dark, our rate equation model predicts no iodine nor FA losses in the dark (orange curves in Fig. 2b and c). However, the iodine and FA content measured by XPS displays a small linear decrease over time in the dark (thick purple and blue curves in Fig. 2b and c). We attribute this decrease to I and FA migration in the dark. To capture this phenomenon, we introduce additional terms into our rate equation model, to take into account ion migration. The chemical rate eqn (5) for the FA time evolution can be re-written as follows:

$$[FA]_t = [FA]_0 + [FAPI]_0(e^{-k_1 t} - 1) + k_3 \times t \quad (7)$$

where k_3 is the FA migration rate. Here, we assume that k_3 is constantly reducing the amount of FA at the surface and that it does not depend on the initial amount of FA. Similarly, to take into account iodine ion migration, eqn (6) can be re-written as:

$$[I]_t = [I]_0 - 3 \times ([Pb(0)]_t - [Pb(0)]_0) + k_4 \times t \quad (8)$$

where k_4 is the iodine migration rate. Positive values for k_3 and k_4 correspond to ion migration from the bulk to the surface of the material (as XPS is sensitive to the topmost 10 nm of the sample), while negative values correspond to either migration from the surface back into the bulk or from the perovskite to the vacuum.

Incorporating these new terms into our rate equation model allows for accurate replication of the experimental data

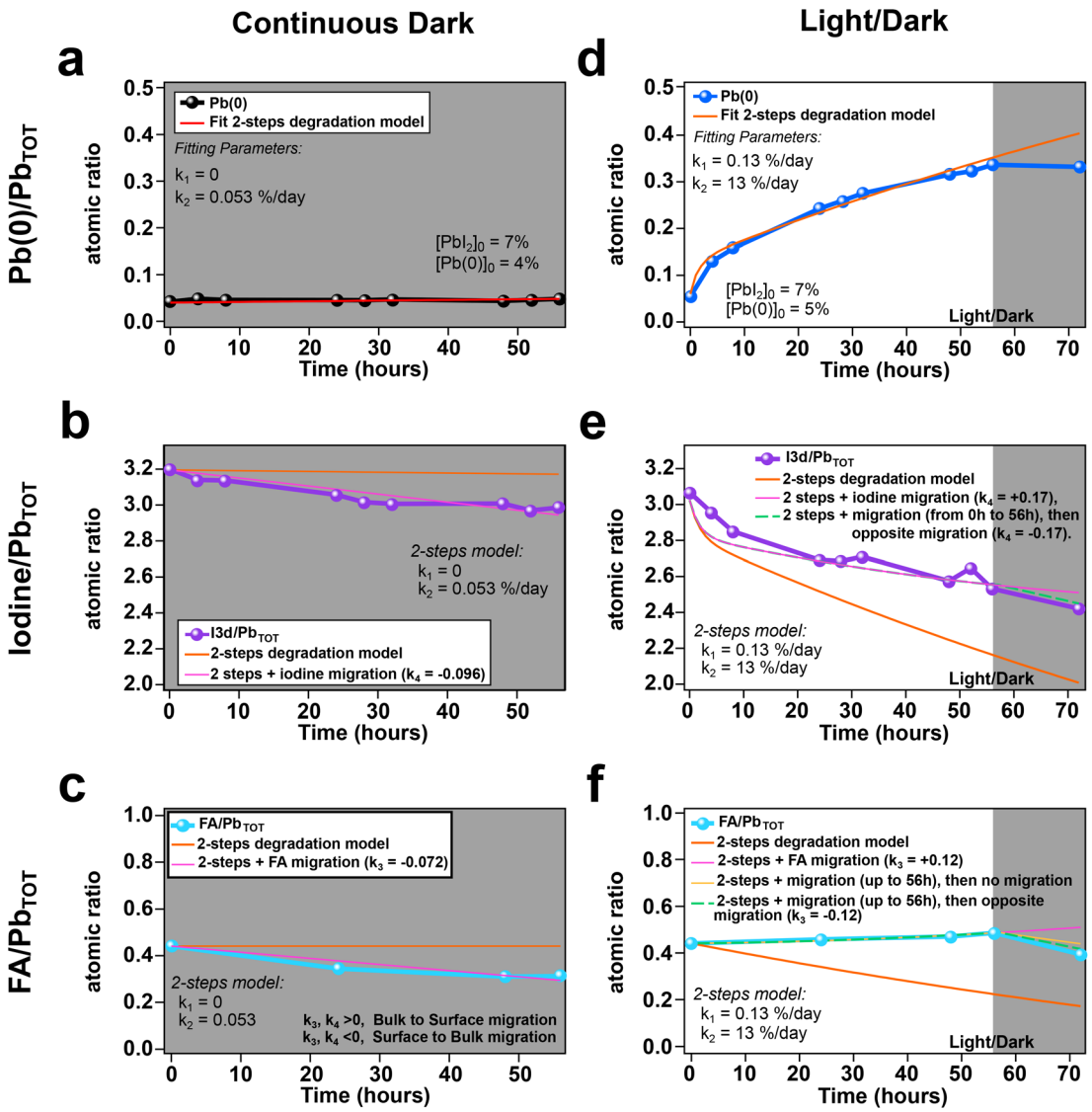

Fig. 2 Modeling the FA and I losses in $Cs_{0.05}FA_{0.85}MA_{0.10}Pb(I_{0.95}Br_{0.05})_3$ perovskite based on Pb(0) generation and the chemical rate equation model: (a–c) time evolution of Pb(0) generation, iodine and FA losses recorded by XPS on a pristine sample kept in the dark and under ultra-high vacuum (UHV) conditions. (d–f) Time evolution of Pb(0) generation, and iodine and FA losses recorded by XPS on a pristine sample under illumination in an ultra-high vacuum (UHV) environment. The gray shadow background corresponds to a time when the sample was kept under dark conditions, while the white background corresponds to a time when the sample was under illumination. The thick dotted solid lines correspond to the amount of Pb(0), I, and FA measured in XPS. The thin orange curves correspond to a pure 2-step degradation model (without any migration), while the magenta, green, and yellow curves correspond to the corrected models taking into account some ion migration in addition to the pure 2-step chemical decomposition model. In each case, the rate of chemical reactions k_1 and k_2 as well as the rate of iodine migration k_4 and the rate of FA migration k_3 are displayed in the inset of the corresponding panels. Migration from bulk to the surface corresponds to positive values of k_3 and k_4, while negative values correspond to migration in the opposite direction. All rates are expressed in % per day.

(magenta curves in Fig. 2b and c). In the dark, it is found that iodine migrates at a slightly faster rate compared to FA. These results are in line with conductivity measurements reported in the literature (*e.g.* higher mobility of iodine as compared to FA).[52]

Fig. 2d–f depict the time evolution of the Pb(0), I, and FA signals recorded by XPS for a perovskite sample exposed to 56 h of continuous light (highlighted with a white background) followed by 16 h of darkness (highlighted with a shaded background) in an ultra-high vacuum environment. The time evolution curves were constructed using the chemical ratios estimated from XPS measurements. Fig. S6† displays some of the representative XPS spectra, measured in an ultra-high vacuum environment. In each case shown in Fig. 2, the experimental data are plotted alongside the results from our rate equation models, both with and without migration correction terms. Our rate equation model reproduces the time evolution of the metallic lead (Pb(0)) in the first 56 h of light exposure very

well, without any migration terms (lead does not migrate). However, as soon as the sample is placed in the dark, the generation of Pb(0) is stopped. As a consequence, the amount of metallic lead measured starts to deviate from our model.

Considering the k_1 and k_2 rates determined from the fit of the Pb(0) data, we can predict the time evolution of iodine and FA in the absence of ion migration (*e.g.* with $k_3 = k_4 = 0$, orange curves in Fig. 2e and f). Based on the high amount of Pb(0) generated under white light, high losses of I and FA are expected. However, we observed significantly lower losses of I and FA than anticipated. Again, this discrepancy can be addressed by accounting for ion migration phenomena. The magenta curves in Fig. 2e,f are the result of the rate equation model corrected with k_3 and k_4 rates for FA and iodine migration, respectively. In this model, k_1 and k_2 were fixed based on the values estimated from the time evolution of Pb(0), while k_3 and k_4 were left as the only free parameters of the fits. Strikingly, it is found that for both I and FA, the migration rates (k_4, and k_3) have a higher magnitude under light than in the dark. More importantly, the migrations occur in opposite directions under light and in the dark. Under illumination, k_3, and k_4 are positive, indicating a migration from the bulk to the surface (magenta curves in Fig. 2e and f). This migration is most probably initiated by the high loss of I and FA at the surface which creates a concentration gradient between the surface and the bulk of the material, with a high concentration of FA and I in the bulk, while the surface is I and FA depleted. We infer that this concentration gradient is the driving force behind I and FA migration. The migration tends to counterbalance the I and FA losses at the surface. As soon as the light is switched off, the degradation stops, and the migration direction is reversed.

From our rate equation model, we learn that even in the absence of degradation, ion migration (I^- and FA^+) is occurring. In addition, under illumination, the migration is reversed to compensate for the I and FA losses due to the photochemical degradation. As we will demonstrate, this model is a powerful tool for gaining a better understanding of the photo-induced chemical degradation of perovskite materials, particularly in tracking the losses of iodine(I) and formamidinium (FA), as a function of Br content and environmental conditions.

2.3 The beneficial effect of Br content on perovskite photochemical stability in UHV

Previous reports in the literature have shown that increasing Br content increases the structural stability of the perovskite due to the stronger bond strength of Pb–Br as compared to Pb–I.[39]

In the following section, we use our chemical rate equation model to determine if increasing the Br content also increases the photo-stability of the perovskite material in a vacuum. To achieve that we design three types of perovskite materials containing 5%, 10%, and 20% of bromine in their composition ($Cs_{0.05}FA_{0.85}MA_{0.10}Pb(I_{1-x}Br_x)_3$).

Fig. 3a–c depict the time evolution of Pb(0) and Pb(2+) under continuous white light illumination for 56 h, for perovskite films containing 5%, 10% and 20% of bromine, respectively. Comparing the amount of photogenerated Pb(0) across the three samples reveals that the sample with higher Br content shows a lower amount of metallic lead for the same duration of light exposure. These results are well reproduced by our rate equation model (red curves in Fig. 3a–c). It is found that increasing the Br content reduces the k_1 rate (speed) drastically, while k_2 is constant for the three types of samples. In other words, increasing Br content does not affect the speed at which PbI_2 transforms into Pb(0), *e.g.* reaction 2. However, higher Br content has a positive impact on the first chemical reaction step (1), where the reaction rate is reduced by one order of magnitude, *i.e.* the conversion of the perovskite into lead diiodide and FAI is slowed down.

The reduced amount of photogenerated Pb(0) signal for higher Bromine content is also accompanied by a strong reduction of the I losses (ESI Fig. S7†). Our photochemical degradation model reproduces the I and FA losses measured by XPS for the three types of samples well. Moreover, the results of the model show that increasing Br content also reduces the migration rate for I and FA. Both the photochemical degradation rate and the rate for I and FA migration are reduced when increasing Br content.

Thus, it is clear from our rate equation model that increasing the Br content not only enhances the structural stability of the perovskite but also boosts its photochemical stability.

This finding is correlated with our AFM topographic images (Fig. 3d–f), where a lower amount of granular structure was observed on the perovskite samples with higher Br content. For the perovskite sample with 5% of bromine, it is found that 33% of the surface is covered with the degraded granular structure after 56 h of light exposure. In contrast, for the 10% and 20% bromine-containing samples, only 6% of the surface is covered with the degraded granular structure after the full 56 h of illumination. Similarly, the work function maps measured by KPFM were found to be less impacted by the 56 h of continuous light exposure for the perovskite sample with high Br content, as compared to the sample containing only 5% Br. After 56 h of light exposure, the KPFM maps show a secondary phase with a lower work function at the same position as the light-induced granular structure observed in AFM. These lower work function domains represent 14% of the perovskite surface for the sample containing 5% of Br. At the same time, it covers only 6 to 7% of the surface for the perovskite sample with higher Br content. Both our rate equation model and our experimental AFM/KPFM measurements suggest that the photo-chemical stability of $Cs_{0.05}FA_{0.85}MA_{0.10}Pb(I_{1-x}Br_x)_3$ perovskite is increased for higher Br content (x).

Using eqn (4), we can estimate the increase in the activation energy of perovskite degradation as a function of the increase in Br. Our analysis revealed that the samples with 10% Br and 20% Br have activation energy barriers that are 46 meV and 73 meV greater, respectively, than that of the 5% Br sample. These results further highlight the enhanced stability against light associated with a higher Br content.

Based on prior research and our findings, we expect that increasing the Br content in $FAPb(I_{1-x}Br_x)_3$ perovskites enhances their structural stability up to approximately 25% bromide incorporation. This trend is supported by

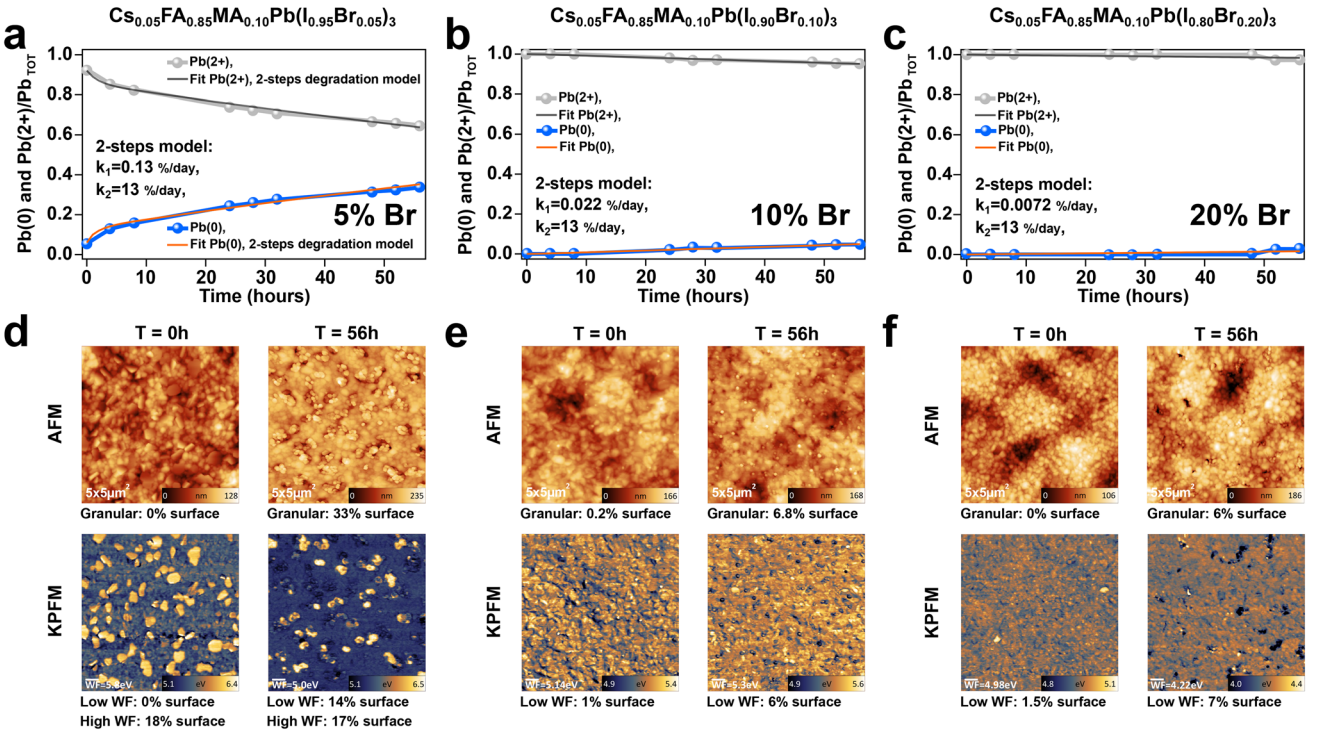

Fig. 3 Increasing the Br content enables the reduction of photo-generated metallic lead Pb(0): (a–c) evolution of the photo-generated metallic lead Pb(0) and pristine Pb(2+) oxidation states in XPS as a function of time for three types of $Cs_{0.05}FA_{0.85}MA_{0.10}Pb(I_{1-x}Br_x)_3$ perovskite samples with 5%, 10% and 20% Br content, respectively. The thick blue dotted solid line corresponds to the photo-generated Pb(0), while the thick gray curve is the Pb(2+) oxidation state of pristine perovskite. The thin orange and black curves correspond to the 2-step chemical reaction rate model. The values for the rate of reactions 1 and 2, namely k_1 and k_2 are depicted in the inset of each panel. A reduction of the k_1 rate as the Br content (x) increases is observed, while k_2 remains constant. (d–f) Topographic AFM images and work function maps measured by KPFM before illumination (T = 0 h), and after 56 hours of continuous illumination recorded for perovskite samples containing 5% Br, 10%, and 20% of Br respectively. The samples with higher Br contents display reduced topographic/work function changes under illumination over time. All rates are expressed in % per day.

experimental and theoretical studies,[39,53,54] which demonstrate that introducing smaller halide ions strengthens Pb-halide bonds, thereby reducing defect formation and the associated release of metallic Pb(0). Our kinetic degradation model, calibrated within the range of 0% to 25% Br, effectively reproduces the observed evolution of Pb(0) and Pb(2+) for the tested compositions. We anticipate that this trend, namely that higher Br content confers improved resistance to photoinduced degradation, can be extended within this compositional window. However, beyond 25% Br, lattice strain and structural instabilities become significant, likely diminishing the stability benefits and necessitating modifications to the current model to account for these effects.

2.4 Impact of environmental conditions on the perovskite photochemical stability

Now that we have successfully used our rate equation model to demonstrate the higher photo-stability of perovskite with higher Br content, we would like to test our model on a photo-degraded perovskite film in distinct environments. In particular, we want to compare the light-induced degradation of a $Cs_{0.05}FA_{0.85}MA_{0.10}Pb(I_{0.95}Br_{0.05})_3$ perovskite film in a N_2 environment *versus* its degradation in ultra-high vacuum (Fig. 4).

For the perovskite kept in N_2 under continuous white light illumination, it is found that the Pb(2+) barely changes over time (gray curve, Fig. 4a), in sharp contrast to the strong decrease in Pb(2+) observed in UHV (purple curve). The sample maintained in an N_2 environment under continuous illumination also exhibited lower iodine losses and an almost constant FA level (Fig. 4b and c).

The absence of a change in the Pb(2+) state of the perovskite in an N_2 environment could be attributed to either increased stability of the perovskite in N_2 (as frequently mentioned in the literature) or the absence of PbI_2 dissociation into metallic lead (Pb(0)), while the perovskite still degrades but in another Pb(2+) component. In either scenario, this suggests that for the sample maintained in N_2, the second reaction step in our rate equation model does not occur, meaning the rate constant k_2 = 0 (Fig. 4d). The absence of Pb(0) generation prevents us from getting a reasonable value for the rate k_1 of the first reaction step when fitting the XPS data results.

To circumvent this issue, we performed AFM/KPFM measurements to verify if degradation of the perovskite occurs in N_2 under continuous light, and to extract a reliable value of k_1, as shown in Fig. 4e–g. Fig. 4e and f present the comparison of the AFM topographic and KPFM work function maps

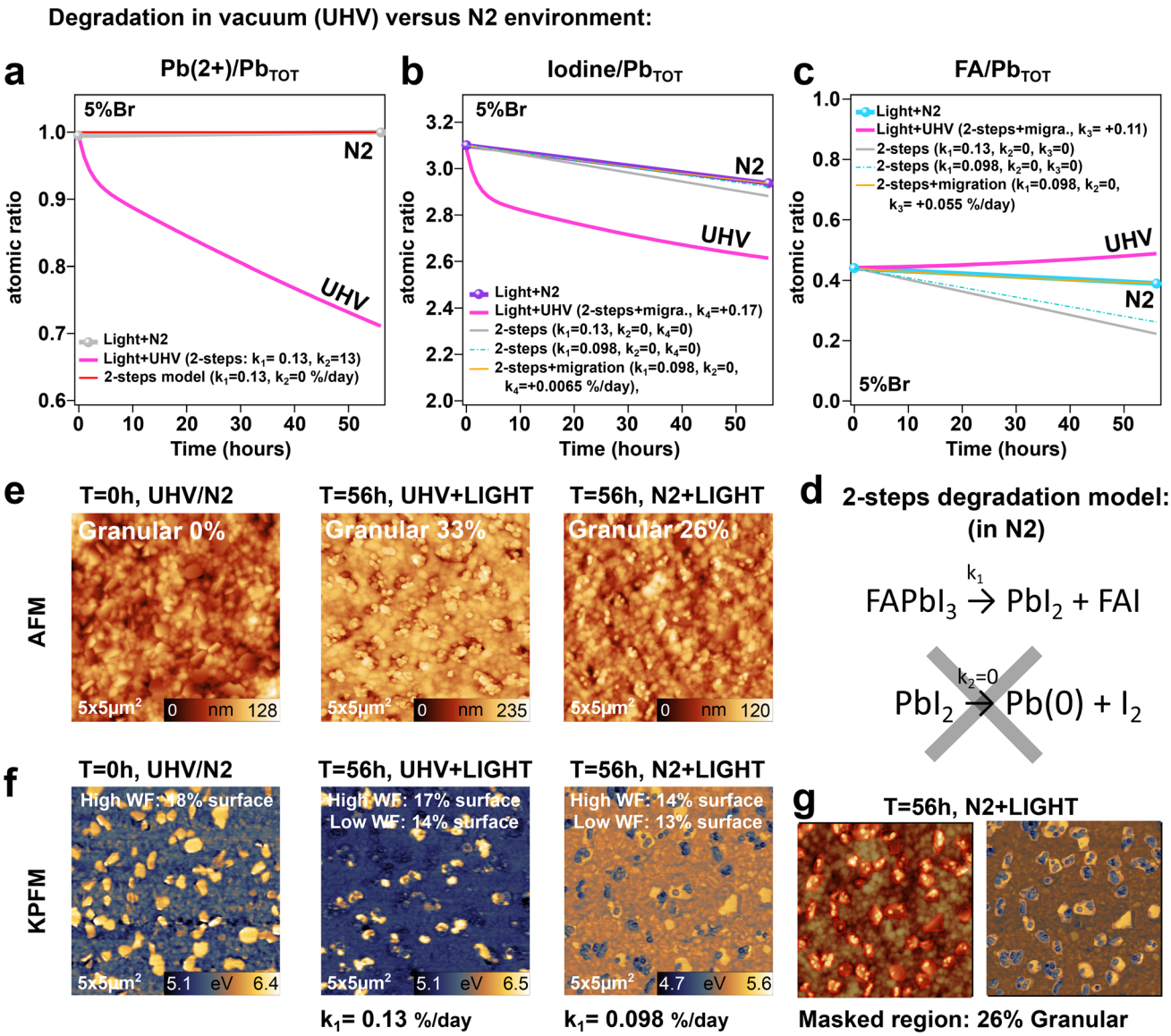

Fig. 4 Impact of the environmental conditions on the perovskite photo-chemical degradation path: a revised 2-step degradation model in N_2. (a–c) Time evolution of the Pb(2+), I, and FA contents recorded by XPS for a $Cs_{0.05}FA_{0.85}MA_{0.10}Pb(I_{0.95}Br_{0.05})_3$ perovskite sample (*e.g.* with 5% Br) kept in an N_2 environment under continuous white light illumination (thick grey, purple and blue curves, respectively). For an easy comparison, the evolution of Pb(2+), I, and FA contents in ultra-high vacuum (under illumination) is also depicted in the same graph as a thin magenta line, labeled UHV. The absence of photo-generated Pb(0) in the N_2 environment, emphasizes the importance for a revised photo-chemical reaction path in the nitrogen environment. (d and e) Topographic AFM image and work function KPFM maps obtained for a pristine perovskite film (with 5% Br) and after 56 h of light illumination in ultra-high vacuum (UHV) and a N_2 environment. Granular structures are still visible in the AFM image after 56 h of light exposure in a N_2 environment, despite the absence of Pb(0) in the XPS, demonstrating that the sample is still degrading in N_2. (f) Revised photo-chemical degradation path in a N_2 environment. (g) AFM and KPFM images with the masked region used to determine the revised k_1 rate for the photo-degradation in N_2. All rates are expressed in % per day.

measured for a pristine $Cs_{0.05}FA_{0.85}MA_{0.10}Pb(I_{0.95}Br_{0.05})_3$ perovskite film, as well as for a light-degraded film in UHV, and a light-degraded film in N_2. In contrast to the pristine case, it is found that both the light-degraded samples in UHV and in N_2 present the same granular structures due to light exposure despite the absence of metallic lead in XPS for the sample degraded in N_2. As discussed earlier in this work and in our previous publication,[46] the granular structures are associated with light-induced photochemical degradation of the perovskite into PbI_x domains (with $x < 2$).

From these observations, we infer that the perovskite film kept in N_2 did degrade under white light illumination, following a similar degradation path to the sample kept in UHV with a non-zero k_1 rate (rate eqn (1) is valid), except that no metallic lead is produced afterward ($k_2 = 0$). It is important to note that we did not observe any increase in oxygen content during the 56 hours of light exposure in the glovebox (Fig. S8†), which rules

out the possibility of oxidation of the metallic lead due to residual oxygen in the glovebox.

An effective method to reliably estimate the k_1 value for the sample degraded in N_2 is to compare the percentage of the surface covered with the granular structure after 56 hours of illumination for both the N_2 and UHV samples. In the UHV case, 33% of the surface is covered by the granular structure after 56 h of illumination, compared to about 26% for the light-degraded sample in N_2 (masked region: Fig. 4g). This observation leads us to suspect that the rate k_1 is slightly lower for the sample degraded in N_2 as compared to the one degraded in UHV. The rate of the photochemical degradation step 1 is known for the light-degraded sample in UHV ($k_1 = 0.13\%$/day, Fig. 1). By assuming that the granular structures are exclusively related to step 1 of the rate equation, we can estimate the rate for the sample degraded in N_2 as follows:

$$k_1|_{N_2} = \frac{26}{33} \times k_1|_{UHV} = 0.8 \times k_1|_{UHV} \quad (9)$$

From eqn (9), we estimate the rate eqn (1) for the light-degraded sample in N_2 to be $k_1 = 0.098\%$ per day. Based on this rate value, it is now possible to fit the iodine and FA losses measured by XPS for the sample degraded in N_2 with our rate equation model ($k_1 = 0.098\%$ per day, and $k_2 = 0$). The result of the fit (without ion migration) is depicted in Fig. 4b and c by the dashed green curves. It is observed that the fit to the curve considering the rate k_1 estimated from the granular structure, reproduces the experimental data of the measured iodine losses in N_2 well, without the need to consider ion migration.

To properly describe the FA losses, however, a small migration rate term needs to be taken into account (orange curve in Fig. 4c). This term enables us to account for the higher amount of FA measured as compared to the one we would expect from eqn (1) of the rate equation model. The rate of FA migration from bulk to the surface is $k_3 = +0.048\%$ per day, which is about 3 times lower in magnitude with respect to the migration we observed for the sample exposed to light in UHV (Fig. 2f).

Therefore, our rate equation model was successfully employed to characterize the light-induced photochemical degradation of the perovskite in an N_2 environment. Our AFM/KPFM images allowed us to ascertain that the sample degraded in N_2 under illumination, enabling us to estimate a meaningful reaction rate k_1. We also demonstrated that in N_2, the light degradation does not produce metallic lead, in sharp contrast to what is observed for the sample degraded in a vacuum. It was shown that FA and I migration rates are much lower in the sample degraded in N_2 than the one in a vacuum.

In addition, we applied the same rate equation model to analyze the light-induced degradation of the perovskite material in a N_2 environment for the two other perovskite samples containing a higher Br content, namely $Cs_{0.05}FA_{0.85}MA_{0.10}Pb(I_{0.90}Br_{0.10})_3$, and $Cs_{0.05}FA_{0.85}MA_{0.10}Pb(I_{0.80}Br_{0.20})_3$. The results of this analysis are depicted in ESI Fig. S9.† Following the same procedure as the one described earlier for the 5% Br sample, the k_1 rate values of the 10% and 20% Br-containing sample were extracted by applying a mask to the AFM/KPFM data, to determine the surface area covered with granular structures after 56 h of continuous light exposure (Fig. S10 and S11†).

The light degradation in a N_2 environment of the 10% and 20% Br-containing sample shows a similar trend to the 5% Br sample. In all three cases, the second step (reaction 2) of the photochemical degradation is absent ($k_2 = 0$). Moreover, all samples present a non-zero k_1 rate. However, the k_1 rates were found to be lower in N_2 as compared to the UHV case. More importantly, the photochemical degradation seems to be partially quenched for the sample with higher Br content, as shown by their much lower k_1 rates. Furthermore, most of the ion migration is suppressed for the sample with 10% and 20% of bromine. Once again, our rate equation model enables us to picture the highest photostability of the perovskite materials in N_2 environments, and allows for a correct modeling of the FA and I losses for three types of perovskite samples. In particular, it demonstrates that samples with higher Br content are generally more stable against light exposure.

Fig. 5 summarizes the main findings of this study. Under continuous dark conditions, there was no metallic lead recorded in the XPS in both UHV and N_2 environments (Fig. 5a and Table II of the ESI†). Additionally, the AFM and KPFM images of the sample kept in the dark in the UHV for 56 h display the same topography and work function characteristics as the freshly grown pristine perovskite film, without any granular structure at the surface (Fig. S12†). These findings let us conclude that there is no degradation of the perovskite in the dark in both N_2 and UHV environments ($k_1 = k_2 = 0$).

As soon as light shines on perovskite in a UHV environment, a photochemical degradation takes place, leading to the appearance of a Pb(0) signal in the XPS and the formation of granular structures at the surface of the perovskite film as depicted by our AFM/KPFM measurements. This degradation can be accurately described by the rate equation model depicted in Fig. 5b. Our model demonstrates that the degradation also leads to FA and I migration from bulk to the surface. This phenomenon occurs in order to compensate for the depletion of FA and I content at the surface caused by the photochemical degradation (Table III of the ESI†).

In N_2, the light-induced perovskite degradation does not produce metallic lead, in contradiction to the sample degraded in a vacuum (Fig. 5c, and Table IV of the ESI†). The absence of metallic lead makes it more challenging to accurately monitor the reaction rate and the photochemical degradation pathway. Moreover, FA and I migration rates are much lower in the sample degraded in N_2 as compared to the one degraded in a vacuum. These pieces of information are critical for properly analyzing other results in the literature, where there are plenty and diverse protocols for the study of light-induced chemical degradation of the perovskite. Here we show that the signal of metallic lead in XPS is not enough by itself to follow the photochemical degradation of the perovskite. In particular, if the degradation protocol is performed in an N_2 environment, where no Pb(0) is generated, the sample still degrades under light exposure at a very similar k_1 rate. This is what we could observe by AFM/KPFM, with the formation of granular structures under light exposure, independent of the environment

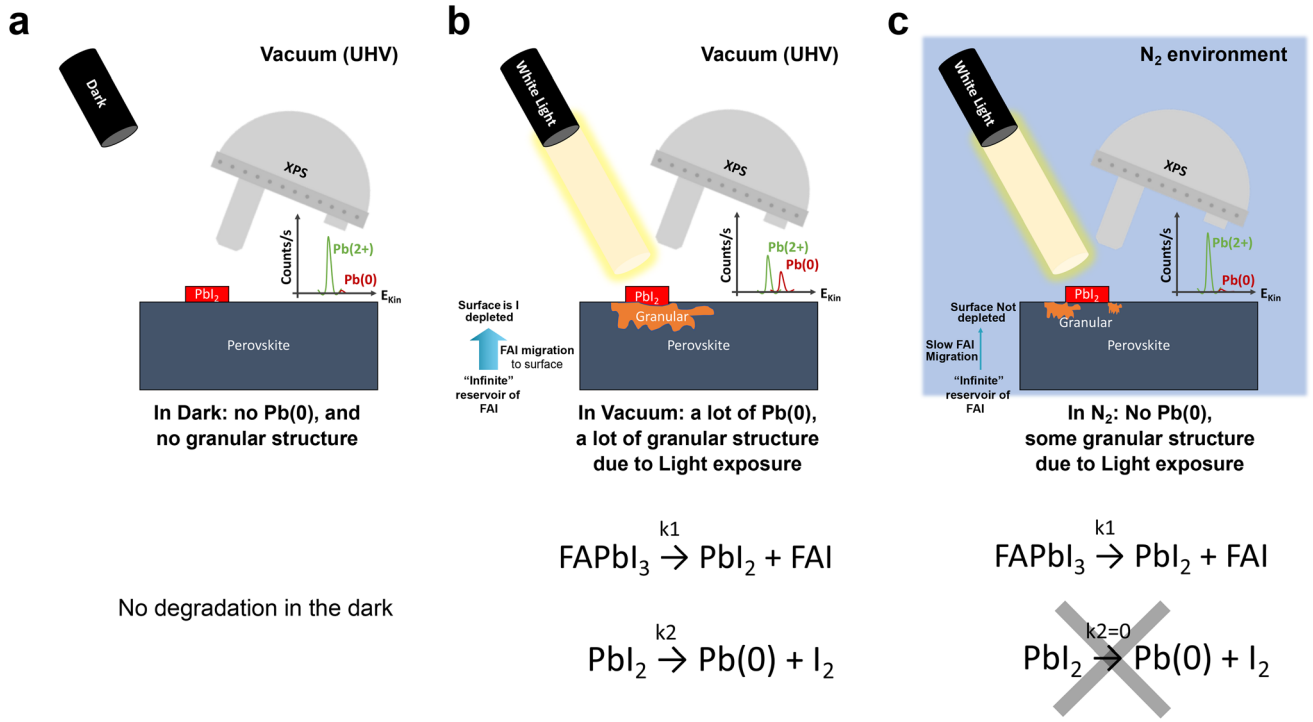

Fig. 5 Schematic illustration of the perovskite photo-degradation in a vacuum and N_2 environment: degradation pathways and associated chemical rate equations. (a) In the dark, no degradation is observed. XPS shows very pure perovskite with the Pb(2+) oxidation state and almost no metallic lead (Pb(0), while AFM and KPFM show well-defined grains with small PbI_2 domains of a higher work function. (b) Under light exposure in vacuum, the perovskite film decomposes, following a 2-step degradation pathway as described by the rate equations. The degradation is at the origin of an increased Pb(0) signal recorded in XPS and of the appearance of small granular structures in the AFM topographic images, with a reduced work function signal. (c) Under light exposure in the N_2 environment, no Pb(0) is measured in XPS, while light-induced granular structures still appear in the AFM/KPFM maps. In N_2 the rate equation needs to be revised, where the second reaction steps producing Pb(0) vanishes.

(*e.g.* both N_2 and UHV). The use of our rate equation model enables us to describe the degradation in a N_2 environment (*e.g.* the FA and I losses), and to demonstrate that that the rate of the first reaction step (eqn (1)) is similar in N_2 and UHV environments. In contrast, the second step of the reaction is quenched in N_2 (Fig. 5c).

Previous reports in the literature have suggested that the photodegradation observed for perovskite in a vacuum could be prevented by simply encapsulating the perovskite in an N_2 environment.[32,34,35,55–58] In contrast, here AFM/KPFM combined with our rate equation model demonstrates that light-induced chemical degradation of the perovskite did occur, even in the inert N_2 environment. The apparent absence of degradation in the XPS analysis is related to a different reaction pathway in a N_2 environment, in which PbI_2 does not convert into Pb(0). XPS is insensitive to the first reaction step of the photodegradation. However, we showed in this study that the granular structure in AFM could be used as a fingerprint of the degradation. This fingerprint enables us to accurately follow the photodegradation and determine the rate of the degradation reaction in the absence of Pb(0) in XPS. Alternatively, our rate equation model could be used to extract the rate of the reaction and migration from the subtle FA and iodine losses recorded in XPS for the light-degraded sample in both N_2 and UHV environments.

Moreover, our rate equation model enables us to investigate in detail the reaction pathway of light-induced degradation in distinct environments and as a function of material composition, particularly as a function of the halide ratio. Previous reports suggested that increasing Br content (<25%) allows for increasing the structural stability of the perovskite. This higher structural stability was attributed to a stronger Pb–Br bond strength with respect to Pb–I.[39] Here, by using our rate equation model we demonstrate that increased Br content also improves the perovskite stability against light, as shown by lower reaction and migration rates. The results of all the fits and the extracted rate values are depicted in Tables V–VII of the ESI.† As a consequence of the slower reaction and migration rates, perovskite films with higher Br content exhibited reduced losses of FA and I, along with greater stability against light exposure.

3 Conclusion

In this study, we developed a rate equation model to thoroughly describe the photo-induced chemical degradation of a state-of-the-art triple cation mixed halide hybrid organic-inorganic perovskite. To check its validity, we tested our model on perovskite films with varying Br contents. We found that perovskite samples containing 10% and 20% Br showed improved stability against light. This result aligns with previous

reports suggesting that incorporating some Br into iodine-based films enhances the structural stability of the perovskite. Finally, we applied our rate equation model to determine the time evolution of FA and I losses under white light exposure in different environments, specifically N_2 and UHV. Our model addresses dissonant results in the literature by demonstrating that light-induced degradation occurs in both N_2 and UHV environments. Subtle differences emerge between the light-induced degradation in these two distinct inert environments. Firstly, the chemical reaction pathway in UHV follows a two-step degradation process with two rate equations, whereas degradation in N_2 is based on a single-step degradation mechanism. We discovered that the initial reaction step, common to both degradations in N_2 and UHV, results in the formation of a granular structure on the perovskite's surface. The second degradation step, which occurs only in UHV, is responsible for the formation of metallic lead in the perovskite film. Secondly, the sample degraded in N_2 showed slower ion migration rates for FA and I. Finally, our chemical rate equation model offers a new tool to track and investigate with great detail the photo-induced I and FA losses in perovskite photovoltaics. This new tool provides new opportunities to gain a deeper understanding of the photochemical degradation process in perovskites and could therefore play an important role in the effort to design a photostable perovskite device.

Data availability

The mathematical derivation of our kinetic model, which is based on a first-order two-step chemical reaction, is fully available in the ESI† of this manuscript. The calculation of the activation energy is also presented in the ESI file.† The fitting of the XPS spectra, used to extract the quantitative ratios of Pb(0)/Pb_{TOT}, I/Pb_{TOT}, and FA/Pb_{TOT}, is included in the ESI.† A detailed methods section explaining the fitting procedure for the XPS data, along with experimental details on the XPS, AFM, and KPFM operating systems, is provided in the ESI.† CasaXPS and Gwyddion[59] software were used for data analysis. Raw and analyzed data will be made available upon request to the corresponding authors.

Author contributions

Jeremy Hieulle designed the experiment, conducted data analysis and XPS measurements, and wrote the manuscript. Hazem Adel Musallam carried out the AFM/KPFM measurements. Anurag Krishna and Tom Aernouts prepared the perovskite sample and conducted the device I–V measurements. Alex Redinger supervised the experimental work at the University of Luxembourg and contributed to the manuscript writing.

Conflicts of interest

The authors state that they have no recognized financial conflicts of interest or personal relationships that could have seemingly impacted the work presented in this paper.

Acknowledgements

This research was funded in whole, or in part, by the Luxembourg National Research Fund (FNR), grant reference [11244141, 13390539, 14757355, and C23/MS/18014671/LION]. A. K. and T. A. acknowledge the financial support by the European Union's Horizon Europe research and innovation programme under grant agreement No. 101147311 of the LAPERITIVO project and grant agreement No. 101120397 of the Approach project. The authors express their gratitude for the technical support provided by B. Uder., U. Siegel, and R. Himelrick.

Notes and references

1 *National Renewable Energy Laboratory NREL Chart*, **https://www.nrel.gov/pv/cell-efficiency.html**, 2024.
2 M. A. Green, E. D. Dunlop, G. Siefer, M. Yoshita, N. Kopidakis, K. Bothe and X. Hao, *Prog. Photovolt.: Res. Appl.*, 2023, **31**, 3–16.
3 J. Zhuang, J. Wang and F. Yan, *Nano-Micro Lett.*, 2023, **15**, 84.
4 R. K. Misra, S. Aharon, B. Li, D. Mogilyansky, I. Visoly-Fisher, L. Etgar and E. A. Katz, *J. Phys. Chem. Lett.*, 2015, **6**, 326–330.
5 D. Wang, M. Wright, N. K. Elumalai and A. Uddin, *Sol. Energy Mater. Sol. Cells*, 2016, **147**, 255–275.
6 X. Guo, C. McCleese, C. Kolodziej, A. C. S. Samia, Y. Zhao and C. Burda, *Dalton Trans.*, 2016, **45**, 3806–3813.
7 A. J. Pearson, G. E. Eperon, P. E. Hopkinson, S. N. Habisreutinger, J. T.-W. Wang, H. J. Snaith and N. C. Greenham, *Adv. Energy Mater.*, 2016, **6**, 1600014.
8 S. Kundu and T. L. Kelly, *EcoMat*, 2020, **2**, e12025.
9 Y. Han, S. Meyer, Y. Dkhissi, K. Weber, J. M. Pringle, U. Bach, L. Spiccia and Y.-B. Cheng, *J. Mater. Chem. A*, 2015, **3**, 8139–8147.
10 Z. Song, C. Wang, A. B. Phillips, C. R. Grice, D. Zhao, Y. Yu, C. Chen, C. Li, X. Yin, R. J. Ellingson, M. J. Heben and Y. Yan, *Sustainable Energy Fuels*, 2018, **2**, 2460–2467.
11 N. H. Nickel, F. Lang, V. V. Brus, O. Shargaieva and J. Rappich, *Adv. Electron. Mater.*, 2017, **3**, 1700158.
12 A. F. Akbulatov, S. Y. Luchkin, L. A. Frolova, N. N. Dremova, K. L. Gerasimov, I. S. Zhidkov, D. V. Anokhin, E. Z. Kurmaev, K. J. Stevenson and P. A. Troshin, *J. Phys. Chem. Lett.*, 2017, **8**, 1211–1218.
13 Y. Li, X. Xu, C. Wang, B. Ecker, J. Yang, J. Huang and Y. Gao, *J. Phys. Chem. C*, 2017, **121**, 3904–3910.
14 K. Oldenburg, A. Vogler, I. Mikó and O. Horváth, *Inorg. Chim. Acta*, 1996, **248**, 107–110.
15 J. Verwey, *J. Phys. Chem. Solids*, 1970, **31**, 163–168.
16 G. I. Gurina, V. D. Evtushenko, A. Y. Kobyakov and V. M. Koshkin, *Theor. Exp. Chem.*, 1985, **21**, 718–719.
17 A. F. Akbulatov, M. I. Ustinova, G. V. Shilov, N. N. Dremova, I. S. Zhidkov, E. Z. Kurmaev, L. A. Frolova, A. F. Shestakov, S. M. Aldoshin and P. A. Troshin, *J. Phys. Chem. Lett.*, 2021, **12**, 4362–4367.
18 I. S. Zhidkov, A. F. Akbulatov, M. I. Ustinova, A. I. Kukharenko, L. A. Frolova, S. O. Cholakh,

C.-C. Chueh, P. A. Troshin and E. Z. Kurmaev, *Coatings*, 2022, **12**, 1–7.
19 B. Charles, J. Dillon, O. J. Weber, M. S. Islam and M. T. Weller, *J. Mater. Chem. A*, 2017, **5**, 22495–22499.
20 D. Zhang, D. Li, Y. Hu, A. Mei and H. Han, *Commun. Mater.*, 2022, **3**, 58.
21 I. Deretzis, A. Alberti, G. Pellegrino, E. Smecca, F. Giannazzo, N. Sakai, T. Miyasaka and A. La Magna, *Appl. Phys. Lett.*, 2015, **106**, 131904.
22 P.-C. Huang, T.-J. Yang, C.-J. Lin, M.-Y. Wang and W.-C. Lin, *Langmuir*, 2024, **40**, 11873–11887.
23 F. Lang, O. Shargaieva, V. V. Brus, H. C. Neitzert, J. Rappich and N. H. Nickel, *Adv. Mater.*, 2018, **30**, 1702905.
24 G. Abdelmageed, C. Mackeen, K. Hellier, L. Jewell, L. Seymour, M. Tingwald, F. Bridges, J. Z. Zhang and S. Carter, *Sol. Energy Mater. Sol. Cells*, 2018, **174**, 566–571.
25 J. M. Azpiroz, E. Mosconi, J. Bisquert and F. De Angelis, *Energy Environ. Sci.*, 2015, **8**, 2118–2127.
26 R. Gottesman, E. Haltzi, L. Gouda, S. Tirosh, Y. Bouhadana, A. Zaban, E. Mosconi and F. De Angelis, *J. Phys. Chem. Lett.*, 2014, **5**, 2662–2669.
27 C. M. Sutter-Fella, Q. P. Ngo, N. Cefarin, K. L. Gardner, N. Tamura, C. V. Stan, W. S. Drisdell, A. Javey, F. M. Toma and I. D. Sharp, *Nano Lett.*, 2018, **18**, 3473–3480.
28 Y. Zhao, P. Miao, J. Elia, H. Hu, X. Wang, T. Heumueller, Y. Hou, G. J. Matt, A. Osvet, Y.-T. Chen, M. Tarragó, D. de Ligny, T. Przybilla, P. Denninger, J. Will, J. Zhang, X. Tang, N. Li, C. He, A. Pan, A. J. Meixner, E. Spiecker, D. Zhang and C. J. Brabec, *Nat. Commun.*, 2020, **11**, 6328.
29 E. T. Hoke, D. J. Slotcavage, E. R. Dohner, A. R. Bowring, H. I. Karunadasa and M. D. McGehee, *Chem. Sci.*, 2015, **6**, 613–617.
30 K. Domanski, B. Roose, T. Matsui, M. Saliba, S.-H. Turren-Cruz, J.-P. Correa-Baena, C. R. Carmona, G. Richardson, J. M. Foster, F. De Angelis, J. M. Ball, A. Petrozza, N. Mine, M. K. Nazeeruddin, W. Tress, M. Grätzel, U. Steiner, A. Hagfeldt and A. Abate, *Energy Environ. Sci.*, 2017, **10**, 604–613.
31 U. B. Cappel, S. Svanström, V. Lanzilotto, F. O. L. Johansson, K. Aitola, B. Philippe, E. Giangrisostomi, R. Ovsyannikov, T. Leitner, A. Föhlisch, S. Svensson, N. Mårtensson, G. Boschloo, A. Lindblad and H. Rensmo, *ACS Appl. Mater. Interfaces*, 2017, **9**, 34970–34978.
32 X. Tang, M. Brandl, B. May, I. Levchuk, Y. Hou, M. Richter, H. Chen, S. Chen, S. Kahmann, A. Osvet, F. Maier, H.-P. Steinrück, R. Hock, G. J. Matt and C. J. Brabec, *J. Mater. Chem. A*, 2016, **4**, 15896–15903.
33 R.-P. Xu, Y.-Q. Li, T.-Y. Jin, Y.-Q. Liu, Q.-Y. Bao, C. O'Carroll and J.-X. Tang, *ACS Appl. Mater. Interfaces*, 2018, **10**, 6737–6746.
34 H.-J. Lin, S. Cacovich, A. Rebai, J. Rousset and C. Longeaud, *ACS Appl. Mater. Interfaces*, 2020, **12**, 19495–19503.
35 R. Guo, D. Han, W. Chen, L. Dai, K. Ji, Q. Xiong, S. Li, L. K. Reb, M. A. Scheel, S. Pratap, N. Li, S. Yin, T. Xiao, S. Liang, A. L. Oechsle, C. L. Weindl, M. Schwartzkopf, H. Ebert, P. Gao, K. Wang, M. Yuan, N. C. Greenham, S. D. Stranks, S. V. Roth, R. H. Friend and P. Müller-Buschbaum, *Nat. Energy*, 2021, **6**, 977–986.
36 E. Smecca, Y. Numata, I. Deretzis, G. Pellegrino, S. Boninelli, T. Miyasaka, A. La Magna and A. Alberti, *Phys. Chem. Chem. Phys.*, 2016, **18**, 13413–13422.
37 T. Sekimoto, R. Uchida, M. Hiraoka, T. Matsui, R. Kikuchi, T. Nakamura, T. Yamamoto, K. Kawano, T. Negami and Y. Kaneko, *ACS Appl. Energy Mater.*, 2022, **5**, 4125–4137.
38 R. K. Misra, L. Ciammaruchi, S. Aharon, D. Mogilyansky, L. Etgar, I. Visoly-Fisher and E. A. Katz, *ChemSusChem*, 2016, **9**, 2572–2577.
39 J. Hieulle, X. Wang, C. Stecker, D.-Y. Son, L. Qiu, R. Ohmann, L. K. Ono, A. Mugarza, Y. Yan and Y. Qi, *J. Am. Chem. Soc.*, 2019, **141**, 3515–3523.
40 S. Singh and E. Moons, *APL Energy*, 2024, **2**, 016112.
41 A. F. Akbulatov, L. A. Frolova, N. N. Dremova, I. Zhidkov, V. M. Martynenko, S. A. Tsarev, S. Y. Luchkin, E. Z. Kurmaev, S. M. Aldoshin, K. J. Stevenson and P. A. Troshin, *J. Phys. Chem. Lett.*, 2020, **11**, 333–339.
42 J. Hieulle, S. Luo, D. Y. Son, A. Jamshaid, C. Stecker, Z. Liu, G. Na, D. Yang, R. Ohmann, L. K. Ono, L. Zhang and Y. Qi, *J. Phys. Chem. Lett.*, 2020, **11**, 818–823.
43 A. Jamshaid, Z. Guo, J. Hieulle, C. Stecker, R. Ohmann, L. K. Ono, L. Qiu, G. Tong, W. Yin and Y. Qi, *Energy Environ. Sci.*, 2021, **14**, 4541.
44 I. S. Zhidkov, D. W. Boukhvalov, A. F. Akbulatov, L. A. Frolova, L. D. Finkelstein, A. I. Kukharenko, S. O. Cholakh, C.-C. Chueh, P. A. Troshin and E. Z. Kurmaev, *Nano Energy*, 2021, **79**, 105421.
45 J. Hieulle, C. Stecker, R. Ohmann, L. K. Ono and Y. Qi, *Small Methods*, 2018, **2**, 1700295.
46 J. Hieulle, A. Krishna, A. Boziki, J.-N. Audinot, M. U. Farooq, J. F. Machado, M. Mladenović, H. Phirke, A. Singh, T. Wirtz, A. Tkatchenko, M. Graetzel, A. Hagfeldt and A. Redinger, *Energy Environ. Sci.*, 2024, **17**, 284–295.
47 E. J. Juarez-Perez, L. K. Ono, M. Maeda, Y. Jiang, Z. Hawash and Y. Qi, *J. Mater. Chem. A*, 2018, **6**, 9604–9612.
48 P. Gratia, G. Grancini, J.-N. Audinot, X. Jeanbourquin, E. Mosconi, I. Zimmermann, D. Dowsett, Y. Lee, M. Grätzel, F. De Angelis, K. Sivula, T. Wirtz and M. K. Nazeeruddin, *J. Am. Chem. Soc.*, 2016, **138**, 15821–15824.
49 X. Zhao, T. Liu, Q. C. Burlingame, T. Liu, R. Holley, G. Cheng, N. Yao, F. Gao and Y.-L. Loo, *Science*, 2022, **377**, 307–310.
50 S. Svanström, A. G. Fernández, T. Sloboda, T. J. Jacobsson, H. Rensmo and U. B. Cappel, *Phys. Chem. Chem. Phys.*, 2021, **23**, 12479–12489.
51 G. Vidon, P. Dally, M. Al-Katrib, D. Ory, M. Kim, E. Soret, E. Rangayen, M. Legrand, A. Blaizot, P. Schulz, J.-B. Puel, D. Suchet, J.-F. Guillemoles, A. Etcheberry, M. Bouttemy and S. Cacovich, *Adv. Funct. Mater.*, 2023, **33**, 2304730.
52 S. Tammireddy, S. Reichert, Q. An, A. D. Taylor, R. Ji, F. Paulus, Y. Vaynzof and C. Deibel, *ACS Energy Lett.*, 2022, **7**, 310–319.
53 A. Aziz, N. Aristidou, X. Bu, R. J. E. Westbrook, S. A. Haque and M. S. Islam, *Chem. Mater.*, 2020, **32**, 400–409.

54 R. K. Misra, L. Ciammaruchi, S. Aharon, D. Mogilyansky, L. Etgar, I. Visoly-Fisher and E. A. Katz, *ChemSusChem*, 2016, **9**, 2572–2577.
55 T. Wang, J. Yang, Q. Cao, X. Pu, Y. Li, H. Chen, J. Zhao, Y. Zhang, X. Chen and X. Li, *Nat. Commun.*, 2023, **14**, 1342.
56 Y. Wang, I. Ahmad, T. Leung, J. Lin, W. Chen, F. Liu, A. M. C. Ng, Y. Zhang and A. B. Djurišić, *ACS Mater. Au*, 2022, **2**, 215–236.
57 Y. Shi and F. Zhang, *Sol. RRL*, 2023, **7**, 2201123.
58 F. Matteocci, L. Cinà, E. Lamanna, S. Cacovich, G. Divitini, P. A. Midgley, C. Ducati and A. Di Carlo, *Nano Energy*, 2016, **30**, 162–172.
59 D. Nečas and P. Klapetek, *Cent. Eur. J. Phys.*, 2012, **10**, 181–188.